



# Elastic contact stiffness and contact resistance for the Weierstrass profile

M. Ciavarella<sup>a,\*</sup>, G. Murolo<sup>a</sup>, G. Demelio<sup>a</sup>, J.R. Barber<sup>b</sup>

<sup>a</sup>*Politecnico di Bari, CEMEC - Centre of Excellence in Computational Mechanics,  
CEMEC-PoliBA-V.le Japigia 182, Bari 70125, Italy*

<sup>b</sup>*Department of Mechanical Engineering, University of Michigan, Ann Arbor, MI 48109-2125, USA*

Received 29 August 2003; received in revised form 10 December 2003; accepted 10 December 2003

---

## Abstract

The Weierstrass series comprises a system of superposed self-affine sine waves that can be used to define a simple idealization of a two-dimensional fractal rough surface profile. The load–compliance relation for the contact of this profile with a rigid plane is here estimated using Westergaard’s solution for the contact of a single sine wave with a plane and various approximations concerning the interaction of the different terms in the series. These approximations are compared with a numerical solution for the contact of the profile defined by the first few terms of the series. Once the load–compliance relation is established, the electrical contact resistance can be determined, using an analogy between the conduction and incremental elastic contact problems. The results show that these simple estimates give quite good predictions of the relations between load, compliance and contact resistance. They also confirm that these relations are largely determined by the coarse scale features of the surface profile, in contrast to the predictions of classical asperity model theories.

© 2003 Elsevier Ltd. All rights reserved.

*Keywords:* Contact resistance; Contact stiffness; Weierstrass profile; Fractal surfaces; Multiscale models

---

## 1. Introduction

Contact between bodies with rough surfaces occurs widely in engineering systems and the micromechanics of the contact process has a profound effect on such

---

\* Corresponding author. Tel.: +39-080-5962811; fax: +39-080-5962777.

E-mail address: [mciava@dimeg.poliba.it](mailto:mciava@dimeg.poliba.it) (M. Ciavarella).

URL: <http://cemec.poliba.it/>

technologically important processes as friction, contact stiffness and electrical contact resistance. Modern surface measurement methods reveal surfaces as multiscale processes with no obvious smallest length scale. For this reason, there has been considerable recent interest in rough surface contact theories based on the representation of the surface as a fractal (Majumdar and Bhushan, 1990, 1991, 1995; Borodich and Mosolov, 1992; Borodich and Onishchenko, 1999; Lopez et al., 1994; Palasantzas and De Hosson, 2003). Seminal work in this area was carried out by Majumdar and Bhushan (1990, 1991, 1995), who argued that the fractal properties of the actual contact areas would be similar to those of the set of islands obtained by slicing through the surface at a constant height. This harks back to the concept of the ‘bearing area’ of a rough surface (Johnson, 1985) and a plausible argument for it can be based on the idea that the resulting microcontacts will be in a fully plastic state and hence can be regarded as analogous to microhardness indentations. It is more difficult to justify for predominantly elastic contacts, though Greenwood and Wu (2001) argue that it provides a first estimate of the location of regions of contact, regardless of the local contact mechanism.

A more convincing approach to the contact of fractal surfaces is to approach the problem iteratively—i.e. to consider first the contact of a ‘truncated’ fractal surface containing a finite number of scales and then explore the incremental effect of adding finer scales, one at a time. The fractal contact problem can then be regarded as the limit of this process as the number of scales goes to infinity. This approach dates back to the seminal paper by Archard (1957), who investigated the first few scales of a surface constructed from spherical asperities superposed on a spherical body. He showed that the relation between total contact area and total load approaches asymptotically to linearity as more scales are added, even though the fundamental contact problem at an individual actual contact is non-linear.

Archard’s method was adapted by Ciavarella et al. (2000) to determine the total actual elastic contact area for a two-dimensional surface defined by the Weierstrass series

$$z(x) = g_0 \sum_{n=0}^{\infty} \gamma^{(D-2)n} \cos\left(\frac{2\pi\gamma^n x}{\lambda_0}\right), \quad (1)$$

where  $\lambda_0$  is the wavelength of the largest scale roughness,  $D$  is the fractal dimension and  $\gamma$  is a parameter defining the inverse ratio between successive wavelengths in the profile. The solution is based on the approximation that the contact pressure at scale  $n$  is equal to the local mean contact pressure at scale  $n + 1$ . In other words, adding an additional scale of roughness does not affect the distribution of pressure at the coarser scales. Of course, we know this is not exactly true. After all, Greenwood and Tripp (1967) showed that the mean contact pressure in a rough Hertzian contact is significantly different from the smooth solution if the surface is sufficiently rough. However, it can be expected to be a reasonable approximation if the fine scale roughness is in some sense sufficiently small and hence if the parameter  $\gamma$  in the Weierstrass series is sufficiently large. Ciavarella et al. (2000) showed that the total actual contact area under elastic conditions is a fractal and reduces without limit as finer and finer scales are added. Thus, the fractal ‘limit’ in this case is an infinite set of point contacts of total measure zero—a result that has also been predicted by direct numerical studies

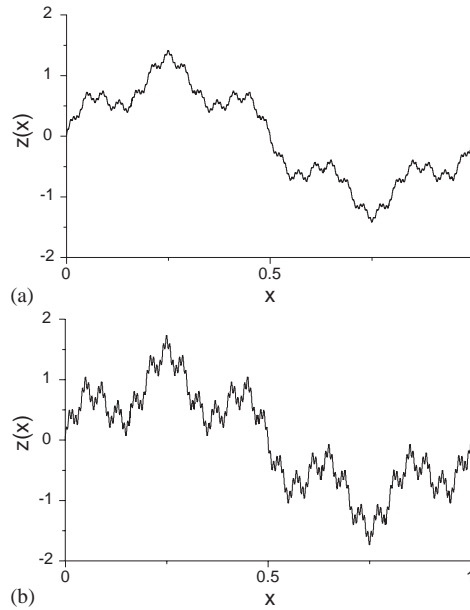


Fig. 1. Typical surface profiles defined by three scales with  $\gamma = 5$  and fractal dimension  $D = 1.25$  (a) and 1.5 (b), respectively.

of the elastic contact problem with progressive mesh refinement by [Borri-Brunetto et al., \(1997\)](#).

The requirement that  $\gamma$  be sufficiently large restricts the ability of the Weierstrass series to represent a realistic rough surface profile. For example, Fig. 1 shows examples of three-scale profiles generated using  $\gamma = 5$  and  $D = 1.25$  and 1.5, respectively. Of course, a similar criticism can be levelled at Archard's original sphere-on-sphere model and other simple multiscale models, such as the self-similar non-convex model of [Borodich and Galanov \(2002\)](#). However, the resulting profiles, though contrived, go some way towards capturing the essential multiscale quality of real profiles.

## 2. Contact resistance and stiffness

[Ciavarella et al. \(2000\)](#) focus on the total actual contact area and the probability distribution for contact pressure, but they do not provide estimates of the stiffness of the contact or the expected value of the electrical contact resistance. These two problems are related, since the boundary value problem for electrical conduction has the same form as that for the incremental elastic contact problem as long as the contacting bodies can be represented by half spaces. In particular, the contact resistance  $R$  is given by ([Barber, 2003](#))

$$\frac{1}{R} = \frac{1}{M(\rho_1 + \rho_2)} \frac{dF}{dh}, \quad (2)$$

where  $F$  is the normal contact force,  $h$  is the normal compliance,  $M$  is a composite elastic modulus given by

$$\frac{1}{M} = \frac{(1 - \nu_1)}{\mu_1} + \frac{(1 - \nu_2)}{\mu_2} \quad (3)$$

and  $\mu_i, \nu_i, \rho_i$  ( $i=1, 2$ ) are the shear modulus, Poisson's ratio and resistivity, respectively, for bodies 1,2.

Traditional treatments of contact resistance regard the contact areas as defining a set of independent constriction resistances in parallel (Cooper et al., 1969). Holm (1958) showed that a single circular contact area of radius  $a$  causes an electrical resistance  $R=(\rho_1 + \rho_2)/2a$ , so for a distribution of such areas  $a_i$ , ( $i=1, N$ ) a simple generalization leads to the expression

$$R = (\rho_1 + \rho_2) \left/ 2 \sum_{i=1}^N a_i = \frac{(\rho_1 + \rho_2)}{2N\bar{a}}, \right. \quad (4)$$

where  $\bar{a}$  is the mean value of  $a_i$ . Fractal contact theories generally predict that the  $N\bar{a}$  is unbounded with progressive scale refinement (Jang and Barber), leading to the rather unlikely conclusion that for a fractal surface, the contact resistance due to surface roughness is always zero. However, this result is disproved by a recent theorem due to Barber (2003), who established finite bounds on the contact resistance for elastic contact of any surfaces that have a highest and lowest point—a condition that is satisfied for the Weierstrass series as long as  $\gamma > 1$ ,  $D < 2$ .

The explanation of this apparent contradiction lies in the fact that actual contact areas for fractal surfaces are likely to be grouped into clusters as a result of the larger scale waves in the power spectral density (PSD). Their electrical resistance is therefore larger than would be obtained if they were widely separated and hence independent. Greenwood (1966) has shown that for a two scale structure comprising a set of  $N$  actual contact areas of radius  $a_i$  clustered within a circular 'contour area' of radius  $b$ , the contact resistance is well approximated by the expression

$$R = (\rho_1 + \rho_2) \left( 1 \left/ 2 \sum_{i=1}^N a_i + \frac{1}{2b} \right. \right) = (\rho_1 + \rho_2) \left( \frac{1}{2N\bar{a}} + \frac{1}{2b} \right), \quad (5)$$

where the second term  $(\rho_1 + \rho_2)/2b$  is the resistance that would be obtained if there were perfect contact over the contour area.

Greenwood's equation provides a good estimate for the contact resistance for a two-scale surface, but it is not readily extended to the multiscale clustering anticipated with real surfaces. Majumdar and Tien (1991) have developed an expression for resistance based on a repeating self-affine pattern of resistances, but the assumed patterns are based on properties of the surface profiles independent of the contact process, except through an estimate of the total actual contact area.

In this paper, we shall extend the arguments of Ciavarella et al. (2000) to estimate the contact resistance and elastic stiffness for the Weierstrass profile. These estimates will be compared with a numerical solution for a truncated series. Barber's bounds theorem (2003) will then be used to place rigorous bounds on the error incurred by neglecting the infinite number of scales beyond any given truncation limit.

### 3. Compliance and resistance for a one-term series

It is convenient to focus on the load compliance ( $F(h)$ ) relation for the rough surface and then make use of analogy (2) to determine the contact resistance. For the simple case where one of the two profiles is plane and the other contains only a single sinusoidal term

$$z(x) = g \cos\left(\frac{2\pi x}{\lambda}\right), \tag{6}$$

the elastic contact problem has been solved in closed form by Westergaard (1939). In particular, full contact is established if the mean pressure

$$\bar{p} > p^* \equiv \frac{2\pi Mg}{\lambda}. \tag{7}$$

For smaller values of  $\bar{p}$ , the contact area semi-width is

$$a = \frac{\lambda}{\pi} \arcsin \sqrt{\xi}, \tag{8}$$

where

$$\xi = \frac{\bar{p}}{p^*}. \tag{9}$$

The contact pressure distribution is given by

$$p(x) = \frac{2\bar{p} \cos(\pi x/\lambda)}{\sin^2(\pi a/\lambda)} \left[ \sin^2\left(\frac{\pi a}{\lambda}\right) - \sin^2\left(\frac{\pi x}{\lambda}\right) \right]^{1/2}, \quad 0 < \xi < 1, \quad -a < x < a$$

$$= \bar{p} + p^* \cos\left(\frac{2\pi x}{\lambda}\right), \quad \xi > 1. \tag{10}$$

Far from the interface  $y=0$ , the two half-planes will be in a state of uniaxial plane strain defined by

$$\sigma_{yy} = -\bar{p}, \quad e_{xx} = e_{zz} = 0. \tag{11}$$

It follows that the relative rigid-body displacement between points at infinity in the two bodies will be unbounded. By the same token, the resistance between points at infinity is unbounded in view of Eq. (2). In order to isolate the additional compliance (and resistance) associated with the surface roughness, we need to take the difference between Westergaard’s solution and state (11). We show in Appendix A that the corresponding value of  $h$  is given by

$$h = g\xi\{1 - \ln(\xi)\}, \quad 0 < \xi < 1$$

$$= g, \quad \xi > 1. \tag{12}$$

The corresponding contact resistance is then immediately obtained from Eq. (2) as

$$\frac{\Delta V}{i} = \frac{1}{M(\rho_1 + \rho_2)} \frac{d\bar{p}}{dh} = -\frac{p^*}{M(\rho_1 + \rho_2)g \ln(\xi)}, \quad 0 < \xi < 1 \tag{13}$$

$$= 0, \quad \xi > 1. \tag{14}$$

#### 4. Simple multiscale estimates

Consider next a two-scale surface comprising only the two terms  $n - 1, n$  in the Weierstrass series. Following Archard (1957) and Ciavarella et al. (2000) we shall assume that the pressure at scale  $n - 1$ , given by Eq. (10) is equal to the mean pressure  $\bar{p}_n$  at scale  $n$ . Thus, if a scale  $n$  asperity peak is located at  $x$ , we can find its contribution to the compliance from Eq. (12), using the scale  $n$  values for  $g, p^*$  and  $\bar{p}_n = p(x)$  from Eq. (10). However, different results will be obtained depending on which asperity is considered. This difficulty is a consequence of the Archard assumption. In reality, there will be some redistribution of the pressure at scale  $n - 1$  so as to equalize the compliance calculated at each contacting asperity.

##### 4.1. The ‘Archard’ approximation

This redistribution typically reduces the mean contact pressure in heavily loaded regions and increases it elsewhere (Greenwood and Tripp, 1967). Thus, an upper limit to the total compliance can be obtained by applying the Archard assumption and focusing on the scale  $n$  asperities near the pressure maxima from scale  $n - 1$ . In other words, we consider locations where the peaks of asperities at scales  $n - 1$  and  $n$  coincide and hence set  $\bar{p}_n = p_{n-1}^{\max}$ . We can then define

$$\zeta_{n-1} \equiv \frac{\bar{p}_n}{p_n^*} = \frac{p_{n-1}^{\max}}{p_n^*} \quad (15)$$

by analogy with Eq. (9), where

$$p_n^* = \frac{2\pi M g_n}{\lambda_n} = \frac{2\pi M g_0 \gamma^{(D-1)n}}{\lambda_0} = p_0^* \gamma^{(D-1)n}. \quad (16)$$

The procedure can then be generalized to permit any number of terms in the Weierstrass series (1).

Ciavarella et al. (2000) showed that  $\zeta_{n-1}$  satisfies the recurrence relation

$$\zeta_n = \gamma^{1-D} f(\zeta_{n-1}), \quad (17)$$

where

$$\begin{aligned} f(\zeta) &= 1 + \zeta, & \zeta > 1 \\ &= 2\sqrt{\zeta}, & 0 < \zeta < 1. \end{aligned} \quad (18)$$

The additional compliance at scale  $n$  is then given by

$$\begin{aligned} h_n &= g_n \zeta_{n-1} \{1 - \ln(\zeta_{n-1})\}, & 0 < \zeta_{n-1} < 1 \\ &= g_n, & \zeta_{n-1} > 1, \end{aligned} \quad (19)$$

where

$$g_n = g_0 \gamma^{(D-2)n}. \quad (20)$$

Eqs. (17) and (18) can be used recursively to define the sequence of values  $\xi_n$  and the total compliance can then be obtained as

$$h = \sum_{n=0}^{\infty} h_n \tag{21}$$

using Eq. (19). This sum is always bounded, since  $0 < h_n \leq g_n$  for all  $n$  and

$$G \equiv \sum_{n=0}^{\infty} g_n = g_0 \sum_{n=0}^{\infty} \gamma^{(D-2)n} = \frac{g_0}{1 - \gamma^{D-2}} \tag{22}$$

is bounded for the admissible values  $\gamma > 1$ ,  $1 < D < 2$ . The quantity  $G$  is in fact half the maximum possible peak to valley roughness of the Weierstrass profile, (assuming that  $\gamma$  is not a rational number, or that the various terms in the series are given random relative phases).

We shall refer to expression (21) and the corresponding estimate of contact resistance from Eq. (2) as the ‘Archard’ approximation.

#### 4.2. Demelio’s approximation

The Archard approximation overestimates the compliance and hence the contact resistance by focusing on locations where peaks at the various scales coincide. An alternative approach is to take an appropriate weighted average of the compliance of the various asperities at each scale. A particularly simple expression of this kind is obtained if we approximate the average compliance over the range of local pressures  $p$  by the compliance of a representative asperity loaded at the mean pressure  $\bar{p}$ —i.e.

$$\overline{h(p)} \approx h(\bar{p}), \tag{23}$$

where the overbar represents the average. If all asperities at the given scale are included (including those that are not loaded), the mean pressure  $\bar{p} = \bar{p}_0$  at all scales and we have

$$h_n = \frac{g_n \bar{p}_0}{p_n^*} \left\{ 1 - \ln \left( \frac{\bar{p}_0}{p_n^*} \right) \right\} \tag{24}$$

for  $\bar{p}_0 < p_n^*$ , from Eq. (A.10) in Appendix A. If  $\bar{p}_0 > p_n^*$ , the  $n$ th scale asperities are completely flattened and  $h_n = g_n$ .

We note from Eq. (16) that  $p_n^*$  increases monotonically with  $n$  and hence if  $\bar{p}_0 < p_0^*$ , Eq. (24) applies at all scales. For this case, the total compliance can be obtained in closed form by substituting for  $g_n, p_n^*$  from Eqs. (16) and (20) and simplifying, giving

$$h_n = \frac{g_0 \bar{p}_0}{\gamma^n p_0^*} \left\{ 1 - \ln \left( \frac{\bar{p}_0}{p_0^*} \right) + (D - 1)n \ln(\gamma) \right\} \tag{25}$$

from which

$$h = \sum_{n=0}^{\infty} h_n = \frac{g_0 \bar{p}_0 \gamma}{(\gamma - 1) p_0^*} \left\{ 1 - \ln \left( \frac{\bar{p}_0}{p_0^*} \right) + \frac{(D - 1) \ln(\gamma)}{(\gamma - 1)} \right\}, \quad \bar{p}_0 < p_0^*. \tag{26}$$

If  $\bar{p}_0 > p_0^*$ , the terms  $n \leq N$  in series (1) will be completely flattened, where  $N$  is the integer part of the expression

$$\frac{\ln(\bar{p}_0/p_0^*)}{(D-1)\ln(\gamma)}$$

These terms will make a contribution to the total compliance, but not to the incremental stiffness or the contact resistance. The remaining terms in the series  $n > N + 1$  are self-affine to the complete series and hence their contribution to the compliance is easily computed by replacing  $g_0, p_0^*$  in Eq. (26) by  $g_{N+1}, p_{N+1}^*$ .

Since this approximation was suggested by G. Demelio, we shall refer to it as the *Demelio approximation*.

#### 4.3. A non-linear layer model

Both of the preceding approximations follow Archard in assuming that the fine scales of roughness have no effect on the mean contact pressure at coarser scales. A method of relaxing this assumption is suggested by Greenwood and Tripp's (1967) solution of the problem of Hertzian contact of rough spheres. They considered the local compliance to be the sum of an elastic displacement due to the mean pressure distribution and a local compliance of the asperities, which they estimated using the Greenwood and Williamson (1966) asperity model theory. In effect, this is a two-scale elastic contact problem, with the Hertzian contact problem being the first scale and the surface roughness being the second (fine) scale. On the fine scale, the mean compliance was determined as a non-linear function of mean contact pressure, so that the problem became equivalent to the contact of two linear elastic bodies separated by a non-linear 'Winkler' foundation—i.e. a layer whose local compliance depends only on local pressure, albeit in a non-linear manner.

This method can clearly be adapted to solve the problem of a two-scale Weierstrass profile, corresponding to any two successive terms of series (1). Furthermore, a numerical investigation of this solution enables us to determine the compliance of this two-scale profile as a function of the global mean contact pressure. This load compliance relation effectively defines the properties of a new non-linear layer representing *two* scales of roughness and we can use these properties to approximate the solution of the *three-scale* problem in which the two scales of roughness are now superposed on a waviness representing the next coarser term in the Weierstrass series. The procedure can then clearly be extended to any number of scales by successive application of the same technique.

### 5. Comparison with numerical solutions

So far we have described various methods of estimating the elastic compliance and hence the contact resistance for a profile represented by a truncated Weierstrass series, but we have not provided any means of assessing their accuracy. The bounds theorem (Barber, 2003) can be applied, based on Westergaard's solution for the first wave of

the series, but the resulting bounds are generally so loose as to include the predictions of all three methods.

However, the bounds would become progressively tighter as more series terms were explicitly included and hence the elastic compliance must be primarily determined by the low-order terms in the series. We can therefore evaluate the various approximations by comparing their predictions with a numerical solution of the contact problem for a truncated series.

### 5.1. The numerical algorithm

For this purpose, a numerical solution was developed based on a discretization of the nominal contact area into  $N$  equal elements. The contact pressure was assumed to be linear in each element. For integer values of  $\gamma$ , series (1) is periodic with wavelength  $\lambda_0$ , so it is sufficient to model one wave of the first term in the series. The shape function for the piecewise linear distribution is the triangular loading of Fig. 5.17(c) of Johnson (1985), for which the displacement is given by Eq. (2.37) of Johnson (1985). The effect of the ‘image’ loads needed to create a periodic sequence can be written down from this equation. In order to avoid an infinite rigid body displacement, it is also necessary to subtract the effect of the mean contact pressure, which is equivalent to a similar sequence of loads uniformly distributed over the wavelength  $\lambda_0$ .

Once the stiffness matrix for the system was constructed from these equations, an iterative algorithm for the unilateral contact problem was developed using the matrix inversion method described in Section 5.9 of Johnson (1985). The algorithm was validated by comparison with Westergaard’s analytical solution. Even with as few as 12 elements, the results agreed closely with the theoretical result from Eq. (12), except at very light loads where only one element is in contact.

### 5.2. Effect of phase

The various terms in the Weierstrass series (1) all peak at  $x=0$ , but a more realistic fractal surface is obtained if random phases are introduced into the various terms. Alternatively, a similar effect could be obtained by examining the function distant from the origin, as long as  $\gamma$  is not a rational function.

The theoretical predictions of Section 4 take no account of the relative phases of the various terms, but the numerical solution clearly depends on the phases selected, so we first examined the effect of relative phase  $\phi$  for a two-scale profile on the load compliance curve. This effect is extremely small at  $\gamma=5$ , so in Fig. 2 we present the curves obtained for various phases for the case  $\gamma=2$ . The scales are normalized with respect to first scale parameters  $p_0^*, g_0$  (To remove the purely geometrical effect of changing phases, we plot the curves in Fig. 2 such that the maxima coincide (the same convention will be used in Figs. 3 and 4). This corresponds to taking reference to the full contact case, rather than the first contact point. Notice that this shift will have no effect on the resistance curves, because they are obtained by differentiation). Also in this figure, we present the average of all the curves which can be seen as an estimate of the ensemble average of a set of random phases. The result lie fairly

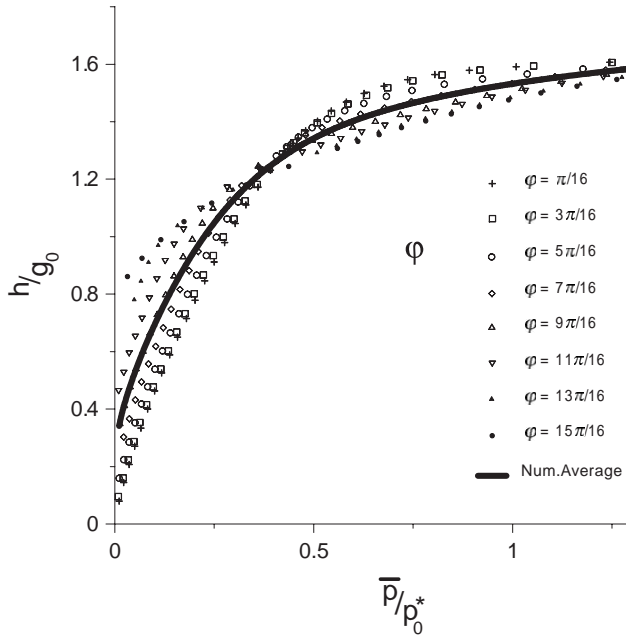


Fig. 2. Effect of relative phase  $\phi$  on the load–compliance curve for a two-scale profile with  $\gamma = 2$  and  $D = 1.25$ . The solid line is the average of the various curves.

close to the average curve for all phases except those close to zero and  $\pi$ , for which the peaks of the two waves are aligned. Since a real surface will have random phases in the various spectral components, we used phase values intermediate between these special cases for all the following tests.

### 5.3. Load–compliance predictions

Fig. 3 compares the three approximate solutions of Section 4 with numerical results for a three-term series and  $D = 1.25, \gamma = 5$ . As expected, the Archard approximation overestimates the compliance at all values of load. The Demelio approximation *underestimates* the compliance at low loads, since in this range a substantial number of fine scale asperities are not in contact, so Eq. (23) underestimates the mean pressure on those that *do* make contact. The non-linear layer model gives good results at low loads, but tends to underestimate the compliance slightly at high loads.

The same comparison is given in Fig. 4 for a three-term series with  $D = 1.5, \gamma = 5$ . The higher fractal dimension means that the higher terms in the series make a larger contribution to the overall process and this generally makes the approximations less accurate. Notice also that the curves continue to rise through larger values of  $\bar{p}/p_0^*$ , since the fine scale waves now require a larger load to achieve full contact. However,

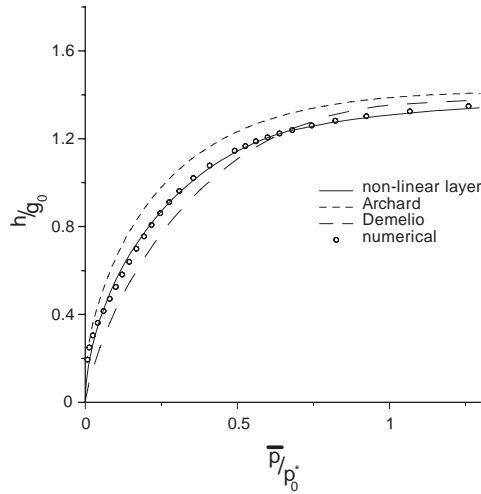


Fig. 3. Comparison of the numerical load–compliance curve with the theoretical predictions of Section 4 for a three-term series with  $D = 1.25, \gamma = 5$ .

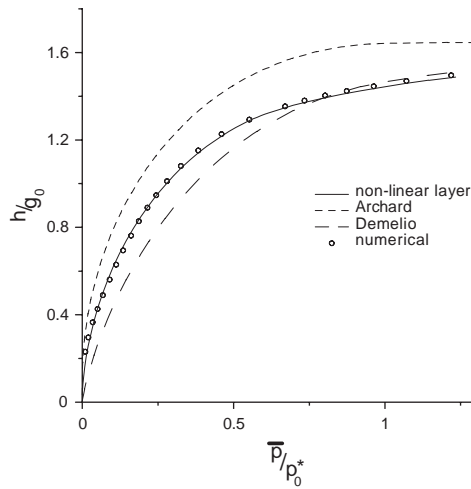


Fig. 4. Comparison of the numerical load–compliance curve with the theoretical predictions of Section 4 for a three-term series with  $D = 1.5, \gamma = 5$ .

the same trends are observed as in Fig. 3 and in particular, the non-linear layer theory still gives quite good predictions throughout the load range.

#### 5.4. Contact resistance predictions

Eq. (2) enables us to deduce the values of contact resistance from the load–compliance curve and results corresponding to Figs. 3 and 4 are shown in Figs. 5 and 6,

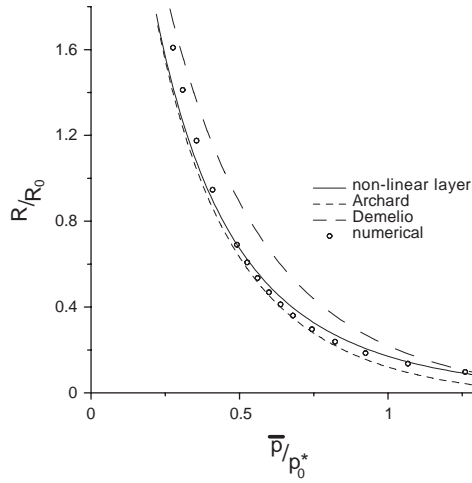


Fig. 5. Electrical contact resistance as a function of load for a three-term series with  $D = 1.25, \gamma = 5$ .

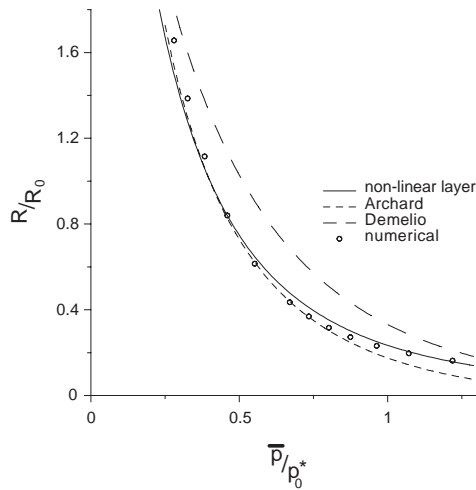


Fig. 6. Electrical contact resistance as a function of load for a three-term series with  $D = 1.5, \gamma = 5$ .

respectively. All the curves show the typical reduction of contact resistance with increasing load. Application of Eq. (2) to the numerical solution requires a process of numerical differentiation, which is therefore rather sensitive to discretization errors. The Archard approximation tends to underestimate the resistance particularly at high loads, whereas the Demelio approximation consistently overestimates by as much as 30%. The non-linear layer theory gives the best predictions overall, the maximum error being about a 12% overestimate at intermediate load ranges.

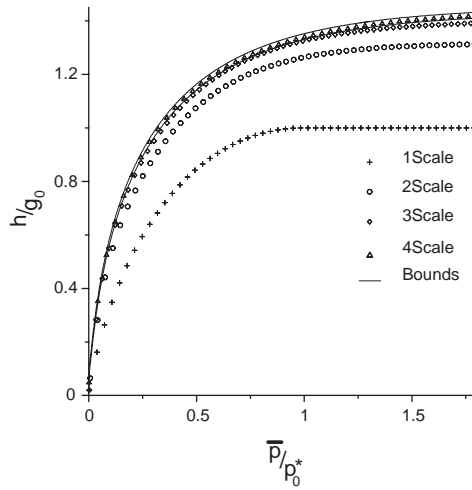


Fig. 7. Effect of additional scales on numerical predictions of contact compliance as a function of load for a truncated series with  $D = 1.25, \gamma = 5$ .

### 5.5. Effect of truncation

Fine scale features can be represented only approximately by a numerical solution and this effectively places limits on the number of terms in the series that can be modeled. Fig. 7 shows the numerical solution for the contact compliance as a function of load for  $D = 1.25, \gamma = 5$  and a truncated series of one, two, three and four terms, respectively. The results certainly suggest that additional fine scale features have a relatively small effect.

Fortunately, the bounds theorem (Barber, 2003) enables us to place rigorous bounds on the additional compliance associated with the infinite number of terms neglected by this truncation. The load–compliance curve for the complete series must lie between the two lines obtained by displacing the truncated load–compliance curve above and below its computed position by a distance equal to the total amplitude of the terms neglected. If only the first  $m$  terms of the series are retained, the total amplitude of the remaining terms is

$$G_m = \sum_{n=m}^{\infty} g_n = g_0 \sum_{n=m}^{\infty} \gamma^{(D-2)n} = \frac{g_0 \gamma^{(D-2)m}}{1 - \gamma^{D-2}}. \tag{27}$$

The corresponding bounds are shown in Fig. 7 for the case where four terms are retained in the series and  $D = 1.25, \gamma = 5$ . The results confirm that the load–compliance relation is largely determined by the coarse scale features in the surface profile.

The corresponding bounds on contact resistance for this case are shown as solid lines in Fig. 8. They are clearly less tight than those on the load–compliance relation, but they still have the benefit of demonstrating that there are no surprises to be expected from the infinite tail of the fractal series.

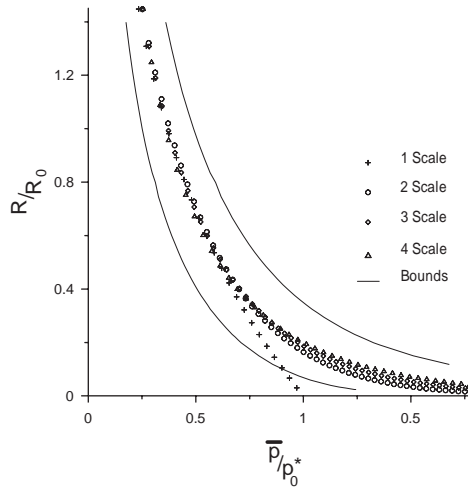


Fig. 8. Effect of additional scales on numerical predictions of contact resistance as a function of load for a truncated series with  $D = 1.25, \gamma = 5$ .

### 5.6. The large $\gamma$ approximation

Real surface profiles have continuous PSDs and representation by a Weierstrass series can be viewed only as a kind of discrete approximation in which the spectral content in a finite band of frequencies is concentrated into a single sinusoid. The approximation can be improved by reducing  $\gamma$ , which has the effect of increasing the number of sinusoids in any given frequency range. However, as explained in the Introduction, the methods proposed here all require some measure of scale separation to give reasonable results, which translates in the case of the Weierstrass series to relatively large values of  $\gamma$ . A similar criticism can of course be leveled at the expressions for total contact area and the probability distribution for contact pressure developed by Ciavarella et al. (2000), but comparison with the numerical results of Borri-Brunetto et al. (1997) shows that the crude approximation implied by  $\gamma = 5$  still captures essential features of the contact process.

## 6. Conclusions

We have developed various methods for estimating the elastic load–compliance relation and the electrical contact resistance for the two-dimensional Weierstrass profile with sufficiently large values of the scaling parameter  $\gamma$ . Comparison with direct numerical solution of the problem for a truncated series profile show that all the proposed approximations give quite good predictions, both for the shape of the resulting curves and for numerical values. The best approximation is that based on the representation of the fine scale roughness as a non-linear elastic layer, as described in Section 4.3. How-

ever, Demelio’s approximation (26) has the major advantage of providing closed-form expressions for both compliance and contact resistance.

Application of the bounds theorem confirms that both relations are largely determined by the first few terms in the series. This agrees with the thinking of Greenwood and Wu (2001) and is in contrast to classical asperity model theories that predict continued change in stiffness and contact resistance as more fine scale features are added.

One referee suggested us that these conclusions may be just relevant to the Weierstrass series fractal, and suggested to look at the profile in Borodich and Galanov (2002). We show in Appendix B that in terms of conductance, we obtain qualitatively similar results, in that an increase of roughness has a non-linear but bounded effect, despite in terms of stress field it may result in an arbitrarily large perturbation.

**Appendix A.**

Westergaard’s solution (1939) for the contact of a rigid sinusoidal rough surface against an elastic half-plane can be expressed in the complex variable form

$$2\mu u_x = (1 - \nu)\Re(\psi) - y\Im(\phi), \tag{A.1}$$

$$2\mu u_y = 2(1 - \nu)\Im(\psi) - y\Re(\phi), \tag{A.2}$$

where  $z = x + iy$  and

$$\phi = \frac{\partial\psi}{\partial z} = -\frac{2\bar{p}\cos\zeta}{\sin^2\zeta} \left\{ \sqrt{\sin^2\alpha - \sin^2\zeta} + i\sin\zeta \right\}. \tag{A.3}$$

In this expression

$$\zeta = \frac{\pi(x + iy)}{\lambda}, \tag{A.4}$$

$$\alpha = \frac{\pi a}{\lambda} \tag{A.5}$$

and the remaining symbols are defined in Section 3.

To evaluate the compliance of the system, we first integrate Eq. (A.3), obtaining

$$\psi = -\frac{\bar{p}\lambda}{\pi} \left\{ \frac{\sin\zeta\sqrt{\sin^2\alpha - \sin^2\zeta}}{\sin^2\alpha} + \arctan \left[ \frac{\sin\zeta}{\sqrt{\sin^2\alpha - \sin^2\zeta}} \right] + \frac{i\sin^2\zeta}{\sin^2\alpha} \right\}. \tag{A.6}$$

After some complex algebra, we then find that at large  $y$ ,

$$2\mu u_y(0, y) \rightarrow -(1 - 2\nu)\bar{p}y - \frac{(1 - \nu)\bar{p}\lambda}{\pi} \{1 - 2\ln(\sin\alpha)\}, \tag{A.7}$$

whilst

$$2\mu u_y(0, 0) = 0. \tag{A.8}$$

The first term in Eq. (A.7) is the displacement associated with a uniform hydrostatic stress  $\bar{p}$  and we need to subtract this to find the additional compliance due to roughness, which is

$$h = \frac{(1 - \nu)p\lambda}{2\mu\pi} \{1 - 2 \ln(\sin \alpha)\}. \tag{A.9}$$

Using Eqs. (8) and (7) to eliminate  $\alpha$ , we have

$$h = g\zeta\{1 - \ln(\zeta)\}, \quad 0 < \zeta < 1, \tag{A.10}$$

where  $\zeta = \bar{p}/p^*$ .

Notice that the maximum compliance due to the roughness is  $g$  and this occurs when  $\bar{p} = p^*$ . For all larger values of  $\bar{p}$ , the compliance remains constant at  $h = g$ , since there is then full contact and only the hydrostatic component of stress changes.

### Appendix B.

#### *B.1. Bounds on compliance and contact resistance for the self-similar contact problem of Borodich and Galanov*

The punch profile in Eq. (20) of Borodich and Galanov is clearly bounded by the expressions

$$\frac{(1 - \varepsilon)r^2}{2R} < f(r, p) < \frac{(1 + \varepsilon)r^2}{2R}. \tag{B.1}$$

It follows from Barber (2000) that the load  $F$  required to produce an indentation  $\zeta$  is bounded by the curves

$$F_1 > F > F_2, \tag{B.2}$$

where  $F_1, F_2$  are the forces required to produce the same indentation for the two bounding surfaces. These are given by the classical Hertzian theory as

$$F_1 = C_1\zeta^{3/2}, \quad F_2 = C_2\zeta^{3/2}, \tag{B.3}$$

where

$$C_1 = \frac{8M}{3} \left( \frac{R}{1 - \varepsilon} \right)^{1/2}, \quad C_2 = \frac{8M}{3} \left( \frac{R}{1 + \varepsilon} \right)^{1/2}. \tag{B.4}$$

Repeating the construction of Fig. 4 of Barber (2003), we find that the slope of the line  $CA$  is

$$\frac{dF}{d\zeta} = \frac{3C_1\zeta_0^{1/2}}{2} \tag{B.5}$$

and hence the equation of this line is

$$F = C_1\zeta_0^{3/2} + \frac{3C_1\zeta_0^{1/2}(\zeta - \zeta_0)}{2}. \tag{B.6}$$

This line will intersect with the curve  $F_1$  when

$$C_2 \zeta^{3/2} = C_1 \zeta_0^{3/2} + \frac{3C_1 \zeta_0^{1/2} (\zeta - \zeta_0)}{2}. \tag{B.7}$$

Dividing by  $C_1/2$  and writing  $x = \sqrt{\zeta/\zeta_0}$ , we then have

$$2\lambda x^3 - 3x^2 + 1 = 0, \tag{B.8}$$

where

$$\lambda = \frac{C_2}{C_1} = \sqrt{\frac{1 - \varepsilon}{1 + \varepsilon}}. \tag{B.9}$$

Eq. (B.8) has two positive roots  $x_1, x_2$  which depend only on  $\varepsilon$ . If we choose the convention that  $x_2 > x_1$ , the larger root  $x_2$  will correspond to the lower bound for the incremental stiffness  $dF/d\zeta$  at the force

$$F = C_2 \zeta^{3/2} = C_2 \zeta_0^{3/2} x_2^3. \tag{B.10}$$

The corresponding bound on the stiffness is given by Eq. (B.5) and we can express this in terms of  $F$  by solving Eq. (B.10) for  $\zeta_0$ , obtaining

$$\zeta_0 = \left( \frac{F}{C_2 x_2^3} \right)^{2/3}. \tag{B.11}$$

Substituting into Eq. (B.5) then yields

$$k \equiv \frac{dF}{d\zeta} = \frac{3C_1}{2x_2} \sqrt[3]{\frac{F}{C_2}}. \tag{B.12}$$

A similar procedure using the root  $x_1$  establishes the upper bounds, so we conclude that the incremental stiffness for the Borodich–Galanov indenter is bounded by

$$\frac{3C_1}{2x_2} \sqrt[3]{\frac{F}{C_2}} < k < \frac{3C_1}{2x_1} \sqrt[3]{\frac{F}{C_2}}. \tag{B.13}$$

The stiffness for a Hertzian indenter of radius  $R$  is given by

$$k_H = \frac{3}{2} \sqrt[3]{FC^2}, \tag{B.14}$$

where

$$C = \frac{8M}{3} R^{1/2}. \tag{B.15}$$

We can therefore normalize bounds (B.13) obtaining

$$\frac{(1 + \varepsilon)^{1/6}}{x_2(1 - \varepsilon)^{1/2}} < \frac{k}{k_H} < \frac{(1 + \varepsilon)^{1/6}}{x_1(1 - \varepsilon)^{1/2}}. \tag{B.16}$$

Thus, the percentage error in incremental stiffness (and hence contact conductance) due to roughness is independent of the load  $F$  and depends only on the roughness parameter  $\varepsilon$ .

From Eq. (B.8) we have

$$\lambda = \frac{3x^2 - 1}{2x^3} \tag{B.17}$$

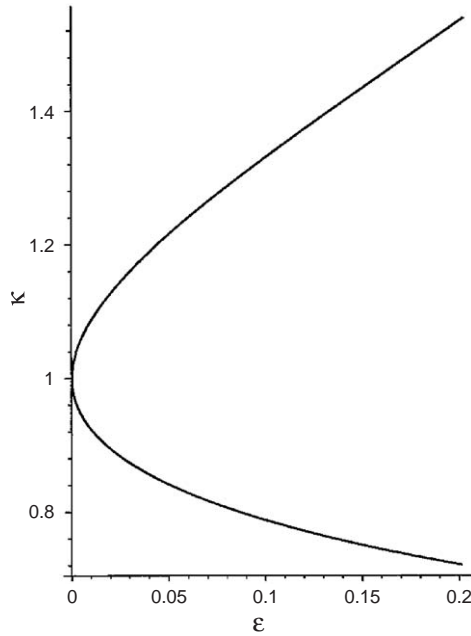


Fig. 9. Bounds on incremental stiffness and contact conductance for the self-similar indentation problem of Borodich and Galanov.

and hence

$$\frac{1 - \varepsilon}{1 + \varepsilon} = \frac{(3x^2 - 1)^2}{4x^6}, \quad (\text{B.18})$$

using Eq. (B.9). Solving for  $\varepsilon$ , we have

$$\varepsilon = \frac{4x^6 - (3x^2 - 1)^2}{4x^6 + (3x^2 - 1)^2}. \quad (\text{B.19})$$

A parametric plot of the two bounds for  $\kappa = k/k_H$  as a function of  $\varepsilon$  is given in Fig. 9.

## References

- Archard, J.F., 1957. Elastic deformation and the laws of friction. *Proc. Roy. Soc. London A* 243, 190–205.
- Barber, J.R., 2003. Bounds on the electrical resistance between contacting elastic rough bodies. *Proc. Roy. Soc. London A* 459, 53–66.
- Borodich, F.M., Galanov, B.A., 2002. Self-similar problems of elastic contact for non-convex punches. *J. Mech. Phys. Solids* 50, 2441–2461.
- Borodich, F.M., Mosolov, A.B., 1992. Fractal roughness in contact problems. *J. Appl. Math. Mech.* 56, 681–690.
- Borodich, F.M., Onishchenko, D.A., 1999. Similarity and fractality in the modelling of roughness by a multilevel profile with hierarchical structure. *Int. J. Solids Struct.* 36, 2585–2612.
- Borri-Brunetto, M., Carpinteri, A., Chiaia, B., 1997. Lacunarity of the contact domain between elastic bodies with rough boundaries. In: Frantziskonis, G. (Ed.), *Probamat 97, Probabilities and Materials*. Kluwer, Dordrecht.

- Ciavarella, M., Demelio, G., Barber, J.R., Yong Hoon Jang, 2000. Linear elastic contact of the Weierstrass profile. *Proc. Roy. Soc. London A* 456, 387–405.
- Cooper, M.G., Mikic, B.B., Yovanovich, M.M., 1969. Thermal contact conductance. *Int. J. Heat Mass Transfer* 12, 279–300.
- Greenwood, J.A., 1966. Constriction resistance and the area of real contact. *Br. J. Appl. Phys.* 17, 1621–1632.
- Greenwood, J.A., Tripp, J.H., 1967. The elastic contact of rough spheres. *ASME J. Appl. Mech.* 34, 153.
- Greenwood, J.A., Williamson, J.B.P., 1966. The contact of nominally flat surfaces. *Proc. Roy. Soc. London A* 295, 300–319.
- Greenwood, J.A., Wu, J.J., 2001. Surface roughness and contact: an apology. *Meccanica* 36, 617–630.
- Holm, R., 1958. *Electrical Contacts Handbook*. Springer, Berlin.
- Jang, Y.H., Barber, J.R., Effect of contact statistics on electrical contact resistance. *J. Appl. Phys.* 94, 7215–7221.
- Johnson, K.L., 1985. *Contact Mechanics*. Cambridge University Press, Cambridge, p. 407.
- Lopez, J., Hansali, G., Le Bossé, J.C., Mathia, T., 1994. Caractérisation fractale de la rugosité tridimensionnelle d'une surface. *J. Phys.* 4, 2219–2501.
- Majumdar, A., Bhushan, B., 1990. Role of fractal geometry in roughness characterization and contact mechanics of surfaces. *ASME J. Tribol.* 112, 205–216.
- Majumdar, A., Bhushan, B., 1991. Fractal model of elastic-plastic contact between rough surfaces. *ASME J. Tribol.* 113, 1–11.
- Majumdar, A., Bhushan, B., 1995. Characterization and modeling of surface roughness and contact mechanics. *Handbook of Micro/Nano Tribology*. CRC Press, New York, pp. 109–165.
- Majumdar, A., Tien, C.L., 1991. Fractal network model for contact conductance. *ASME J. Heat Transfer* 113, 516–525.
- Palasantzas, G., De Hosson, J.Th.M., 2003. Self-affine roughness effects on the contact area between elastic bodies. *J. Appl. Phys.* 93, 898–902.
- Westergaard, H.M., 1939. Bearing pressures and cracks. *ASME J. Appl. Mech.* 6, 49–53.